UNIVERSITY OF LEEDS

This is a repository copy of *Development of flocculation models for improving water treatment*.

White Rose Research Online URL for this paper:
http://eprints.whiterose.ac.uk/149634/

Version: Accepted Version

eprints@whiterose.ac.uk
https://eprints.whiterose.ac.uk/

10TH EUROPEAN WASTE WATER CONFERENCE
DEVELOPMENT OF FLOCCULATION MODELS FOR IMPROVING WATER TREATMENT

Egarr, D. A.[1]*, Horton, L.[1], Rice, H.[2], Hunter, T.[2]

[1] MMI Engineering, Suite 7 Corum 2, Corum Office Park, Crown Way, Warmley, Bristol, BS30 8FJ
[2] University of Leeds, School of Chemical & Process Engineering, Leeds, West Yorkshire, LS2 9JT
* Corresponding Author: Tel. 0117 960 2212   Email: DEgarr@MMIEngineering.com

Abstract

In water treatment the flocculation of particles into larger aggregates or 'flocs' allows impurities or solid material to be removed more easily by sedimentation.

One example is where soluble phosphorus is removed by dosing with ferric sulphate to form a precipitate containing the phosphorus. Dosing usually requires rapid mixing of the ferric sulphate followed by gentle mixing to encourage flocculation.

The use of Computational Fluid Dynamics (CFD) allows multiphase systems to be modelled and the effect of design changes to be studied in order to optimise water treatment. The development of a framework for modelling flocculation provides the possibility to optimise water treatment processes involving the flocculation of particulates.

The paper describes in greater detail the physical models and verification and validation cases undertaken in order to develop the framework and a case study in which CFD was used to optimise the mixing performance of a flocculation tank.

Keywords

Computational Fluid Dynamics, Flocculation, Multiphase, Population Balance Model

Nomenclature

β	Collision frequency	m³/s
n_i, N_i	Number concentration of particle i	#/m³
S_i	Rate of breakup of particle i	1/s
t	Time	s

Introduction

Computational Fluid Dynamics may be applied to calculate the transport of particulates and flocs. This is important in processes where settlement or mixing are of interest. In the treatment of both potable and wastewater, flocculation is a method used to grow particle sizes and therefore enhance settling rates.

Such an example is the dosing of a metal salt such as ferric sulphate into a stream of wastewater, which reacts to form a precipitate containing phosphorous. The precipitate may be removed by gravity settlement downstream. However, optimum removal of the precipitate is achieved with effective flocculation in order to enhance the floc sizes.

Under an Innovate UK project, MMI Engineering has been collaborating with Leeds University and Sellafield Ltd in a project to improve the design of sludge separation and collection systems. MMI's contribution to the project was the development of a framework within a Computational Fluid Dynamics solver that includes flocculation and breakup models for particulates.

This paper describes a summary of the work undertaken and a hypothetical application of the solver to two different flocculation tanks. A case study is also presented, where CFD has been applied to optimise the mixing performance of a flocculation tank.

Methodology

In this work the flocculation solver has been developed using the open source code OpenFOAM v2.2.x. In all cases, the model geometry was generated using ANSYS Design Modeller and the computational mesh generated using ANSYS ICEM.

Population Balance Model

Combining the terms for flocculation and breakup and writing the rate of flocculation in terms of frequency and number concentration, the discretised population balance equation is given by the following equation set (Biggs & Lant, 2002), which describes the modes by which particulate mass may shift in to a given size group by means of flocculation and breakup:
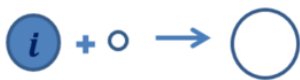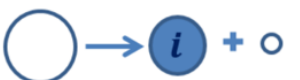
$$\frac{\Delta n_i}{\Delta t} = \sum_{j=1}^{i-2} 2^{j-i+1}\beta_{i-1,j}N_{i-1}N_j + \frac{1}{2}\beta_{i-1,i-1}N_{i-1}^2 \qquad \text{Birth Flocculation}$$

$$-\sum_{j=1}^{i-1} 2^{j-i}\beta_{i,j}N_iN_j - \sum_{j=i}^{N-1}\beta_{i,j}N_iN_j \qquad \text{Death Flocculation}$$

$$+2S_{i+1}N_{i+1} \qquad \text{Birth Breakage}$$

$$-S_iN_i \qquad \text{Death Breakage}$$

Figure 1: Population balance model

Flocculation

Flocculation is brought about by the collision of particles or flocs. There are three modes of flocculation, which are perikinetic (due to Brownian motion), differential settling (due to faster settling particles colliding with slower particles) and orthokinetic (due to velocity gradients i.e. shear, in the flow).

In this work, orthokinetic flocculation is considered to be the dominant mode. Orthokinetic flocculation models are a function of the shear rate. The shear rate may be described by the scalar 'G', which is, in turn, related to the local turbulence in the flow. In addition to flocculation, floc breakup must also be considered, otherwise floc sizes would continually grow in a numerical model. Again, floc breakup models may also be a function of 'G' but also incorporate empirical constants that differ depending on the particulates. Thus, the effect of turbulence promotes flocculation but also induces floc breakup.

As particles collide, the effect of electrostatic attraction and repulsion forces comes into effect. The sum of these two forces as a function of distance generates a curve with a peak repulsion force, known as the energy barrier. This is presented schematically in Figure 2. Provided that the collision energy is sufficient to overcome this barrier, attachment between two particles will occur.

As flocculation requires particle collisions, the more collisions that occur, the greater the chance of flocculation. Thus, residence time, t, is also an important parameter. The product of 'G' and 't' is known as the Camp number and values in the range 10,000 to 100,000 are quoted in the literature (Elmaleh & Jabbouri, 1991) as being optimal for flocculation chambers.
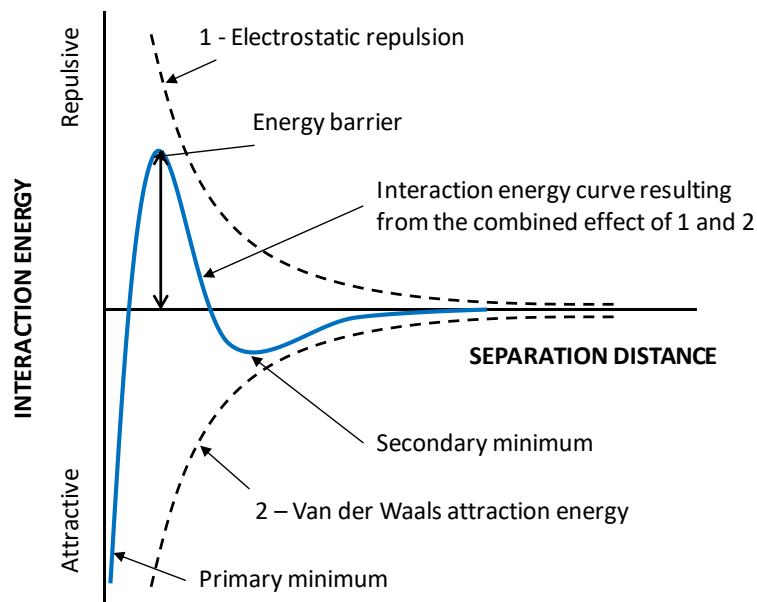
Figure 2: Representation of the DLVO (Derjaguin, Landau, Verwey, and Overbeek) theory. Adapted from Govoreanu (2004).

Settling Behaviour

In comparison to the agglomeration and breakage of gas bubbles within a fluid, flocs of particles generate an additional complexity in that, between the particles, there will be voids of fluid. These voids, which may be referred to as interstitial fluid, result in a floc whose effective diameter is larger than the mass effective diameter i.e. the mass effective diameter is the diameter the floc would have if the voids of fluid were removed. Consequently, the effective mass of the floc is also reduced, which should be given consideration when calculating the particle settling velocity.

Phases of Development

In order to develop the solver, the physical models were implemented and tested in phases. These were:

I.   Settling column to validate the model for settling.
II.   Validation for convective transport against a lab scale settler.
III.   Verification of population balance model against commercial CFD code.
IV.   Hypothetical test case for flocculation and breakup.
V.   Validation of flocculation model against experimental data.

Phases I to IV were considered successful, however, it was found that in Phase V, due to lack of data available to define appropriate boundary conditions, the flocculation solver could not be validated.

Results

Phase I – 1D Settling

A 0.5m internal diameter column, 1.5m in height, was used to measure the concentration of glass beads at discrete points as a suspension was allowed to settle. The water-solids mixture was mixed using a pump in order to try and achieve a completely mixed state prior to the settling test. Schematics of the settling column are presented in Figure 3.

The nominal working volume was 236 litres so that the water level within the column was 1.2m, therefore giving a clearance of 0.3m between top water level and the top of the column.
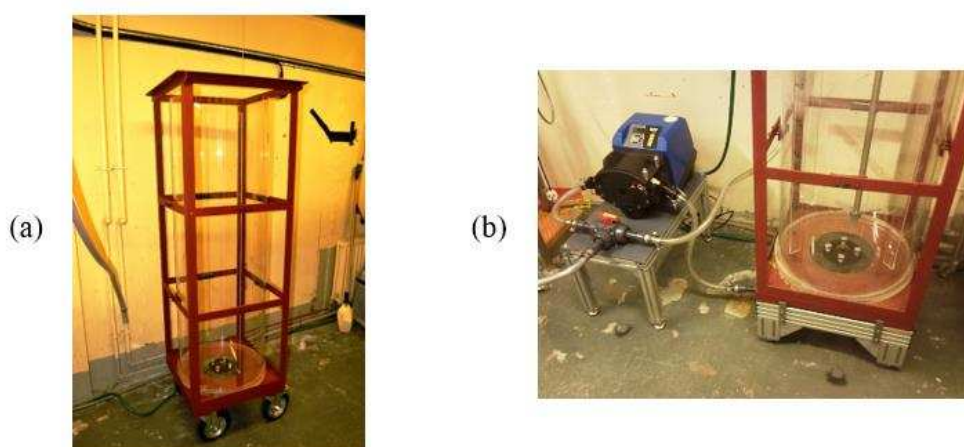
Figure 3: Photographs of settling column (a) prior to full commissioning, May 2013; (b) fully commissioned, with recirculation pump shown, March 2014.

Water was specified with a density of 1000 kg/m^3 and a viscosity of 0.00122 kg/ms based on a fluid temperature of 12.3℃ as measured in the experiments.

The particulates were a mixture of 50% w/w Honite 16 and 50% w/w Honite 22 (Guyson International, UK). The dried solids density was specified as 2460 kg/m^3 for Honite 16 and 2450 kg/m^3 for Honite 22. The Particle Size Distribution (PSD) is presented in Figure 4, with the 50% mixture in red. In the model, 5 scalars were used to represent Honite 22, which were discretised from the PSD in blue and 5 scalars were used to represent Honite 16, which were discretised from the PSD in orange.
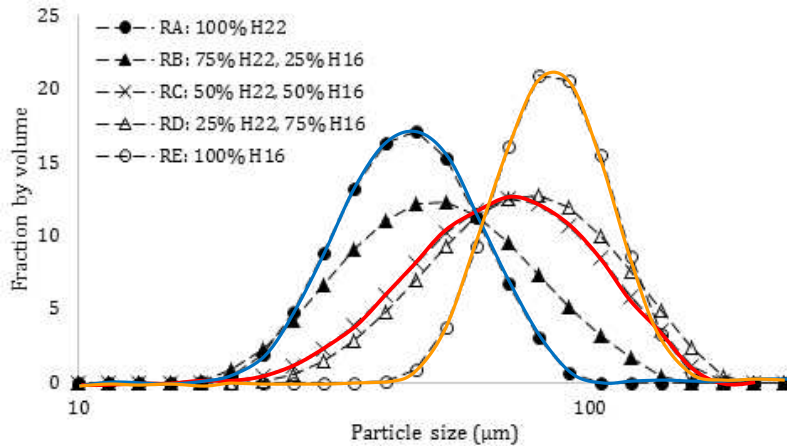
Figure 4: PSD for Honite spherical glass particles. "H22" refers to Honite 22, "H16" to Honite 16. RA to RE are runs A to E with varying combinations of H22 and H16 by mass.

The ten slip scalars were each modelled with a slip velocity based on the settling of spherical particles for the free settling regime only.

Results for the total solids mass fraction at the sampling points are presented in Figure 5 with comparison to the experimental measurements. The CFD results compare well, providing confidence that the CFD model can calculate 1D settling. Differences between the results may be due to incomplete homogeneity of the solids at the start of the test due to the efficiency of the impeller. Additionally, in the CFD model, it was assumed that, at the start of the test, the fluid was stationary, whereas in reality there would have been residual swirl once the impeller was switched off.
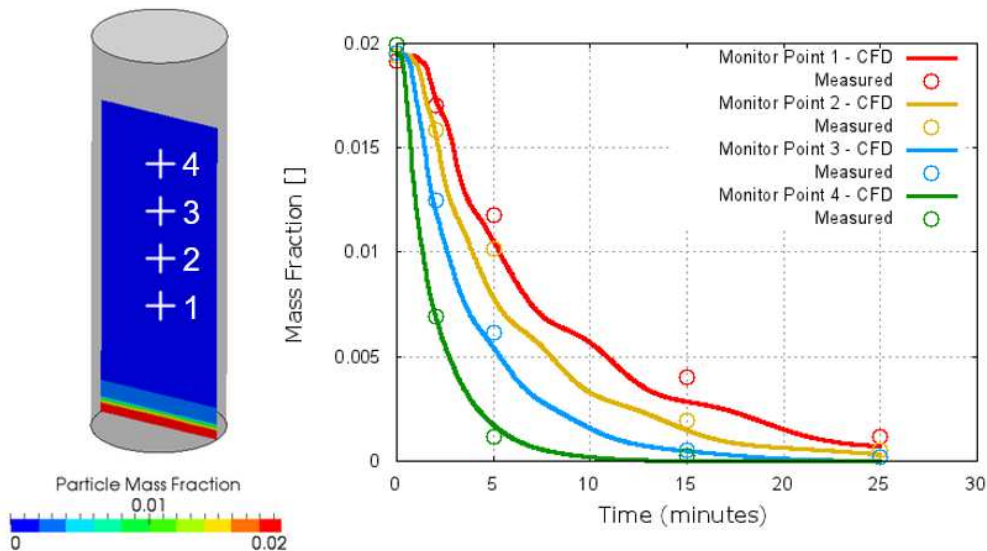

Figure 5: Comparison of total solids mass fraction at the sampling points between CFD and measurements. Figure to left shows position of monitor points and the calculated concentration distribution at the end of settling.

Phase II – Convective Transport in Settler

The geometry of the laboratory scale clarifier of Krebs (Krebs, et al., 1998) is presented in Figure 6. The flow carrying glass beads enters the clarifier at the full-width inlet slot and particulates are allowed to fall out on to a honeycomb array, where they become trapped. The clarified flow exits through the weir on the right.

The CFD model built for the purpose of this study is restricted to the area marked in red, with a desludging boundary prescribed at the bottom of the tank. For the purpose of reducing the grid size, the geometry was assumed to be 2-dimensional as this was appropriate for the geometry of the tank.
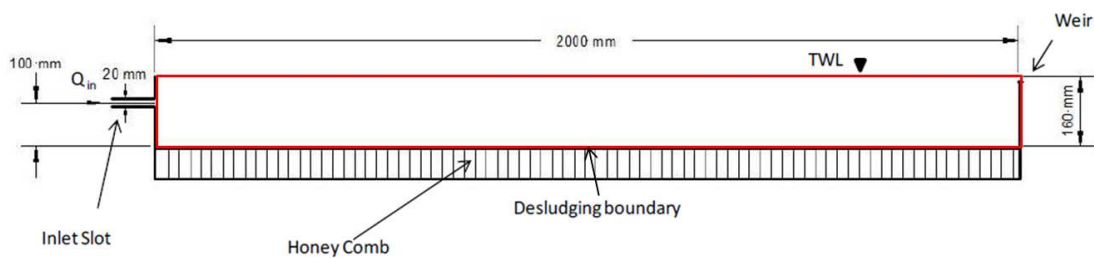
Figure 6: The geometry of the laboratory scale clarifier of Krebs (Krebs, et al., 1998).

Water was specified with a density of 999.3 kg/m^3 and a viscosity of 0.00112 kg/ms, corresponding to a water temperature of 15℃. The density of the solids (glass beads) was set to 2500 kg/m^3.

The cumulative Particle Size Distribution (PSD) of the particulates was reduced from 13 size groups down to 10. The 3 size groups that were not represented account for less than 0.5% of the total mass and it was therefore considered that the effect of omitting these size groups would have negligible effect on the results. The PSD is presented in Figure 7. The mean diameter for each group is marked on the x-axis.
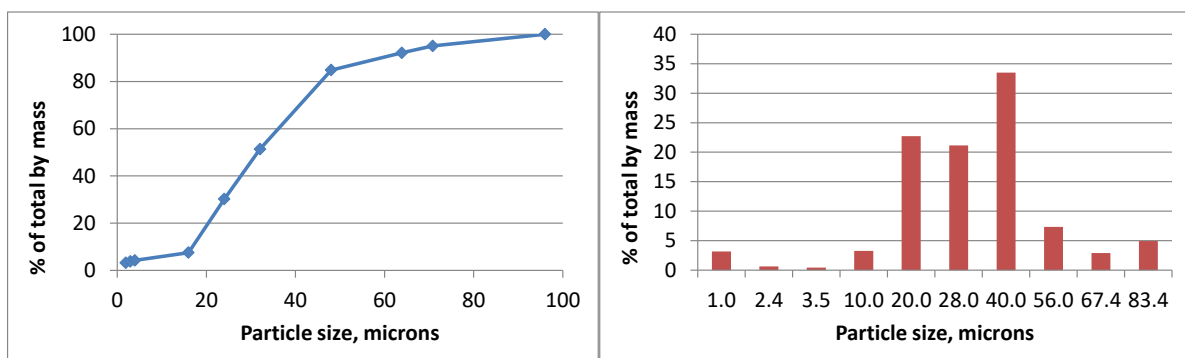
Figure 7: PSD used in the Krebs clarifier calculations.

Contour plots of solids concentration are presented in Figure 8 for the CFX and OpenFOAM results, with both codes showing similar distribution of solids.

Figure 9 presents a comparison of measured concentration profiles between OpenFOAM and CFX at different locations within the tank. These locations are marked in Figure 8, where L [m] denotes the length of the tank and x [m] is the distance from the left-hand side of the tank (where the inlet is located) to the desired location. In general, the OpenFOAM results show a good comparison to both the CFX results and the experimental data.
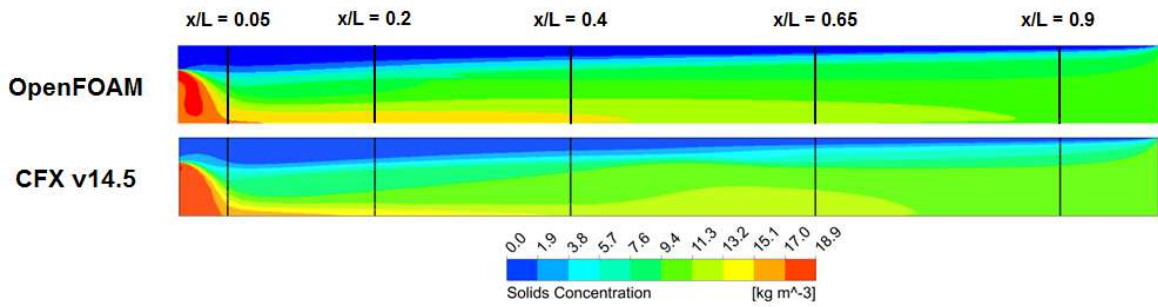
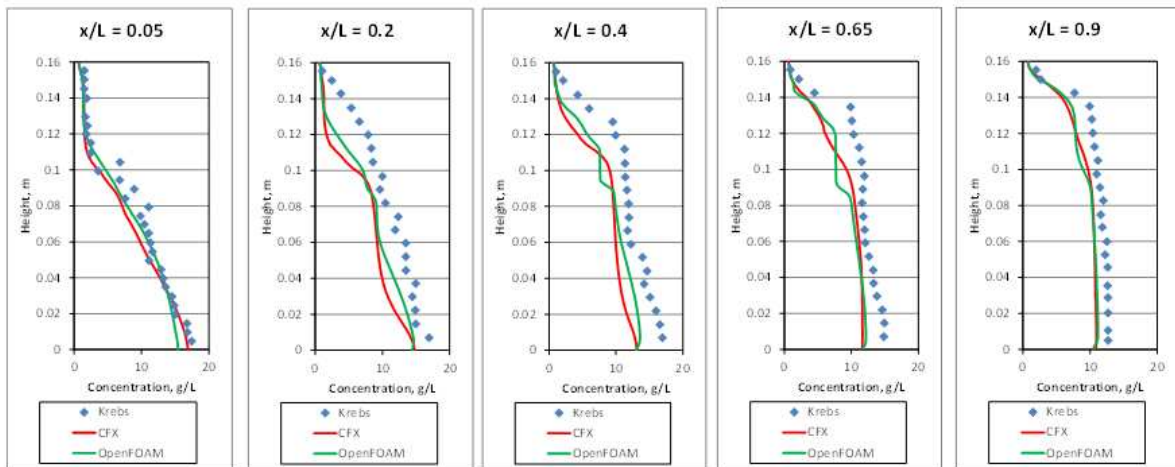**Figure 8: Comparison of contour plots from CFX and OpenFOAM.**

**Figure 9: Comparison of measured solids concentration profiles against CFX and OpenFOAM.**

Phase III – Implementation of Population Balance

A 1D settling column was modelled with water specified with a density of 1000 kg/m^3 and a viscosity of 0.00131 kg/ms. Five particle size groups were included with slip velocities of 0.00176 m/s, 0.00258 m/s, 0.00369 m/s, 0.00514 m/s and 0.00697 m/s, respectively. The density of the particulates was specified as 1005 kg/m^3. A model was not used to represent the thickening effect of the water-solids mixture as the solids concentration increased as this was not considered necessary for the purpose of this calculation. The collision frequency was set to a constant value of 1x10^{-7} #/m^{3}s. The collision efficiency was taken to be equal to 1 and there was no breakup in this case. A comparison was made to results using ANSYS Fluent.

The results for the settling column are presented in Figure 10. The results obtained using OpenFOAM compare fairly well to those from Fluent. There are some differences in the velocity field at the bottom of the settling column, towards the end of the 100 seconds of simulation. This causes slight differences in the solids concentration, which are evident in the contour plots.

From Figure 11, it can be seen that the mass of particulates in each size group is very similar and that, because there is no breakup model, mass migrates to the largest particle group. Differences are assumed to be attributable to the slight difference in concentration field resulting in slightly different flocculation rates.
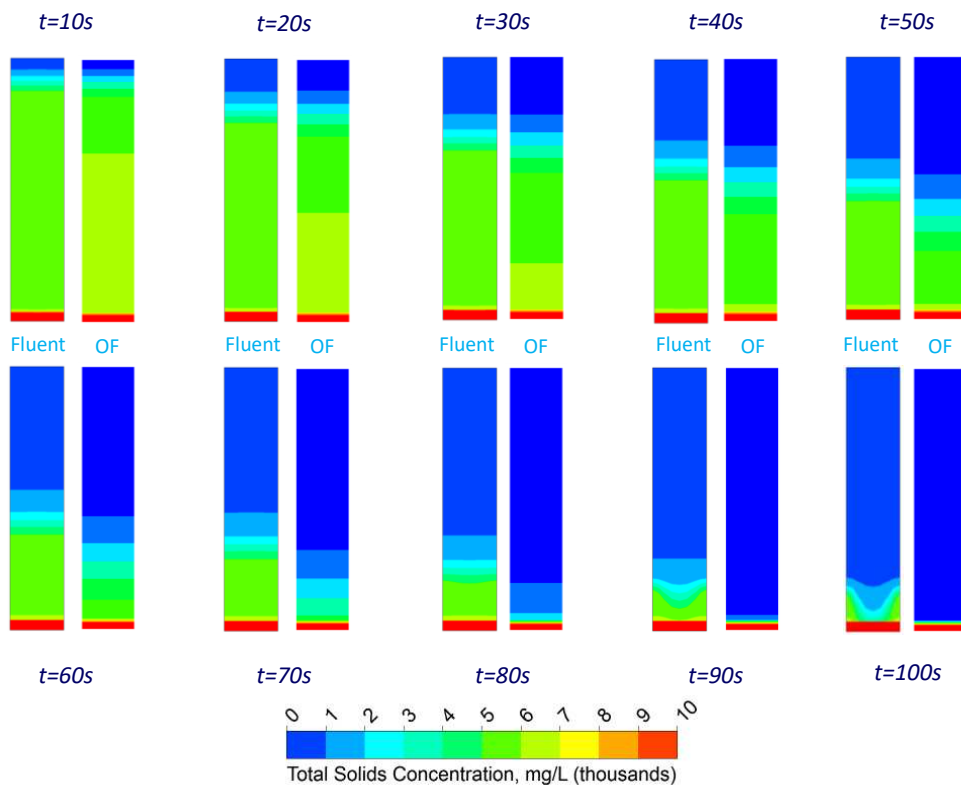
**Figure 10 - Contours of total solids concentration.**
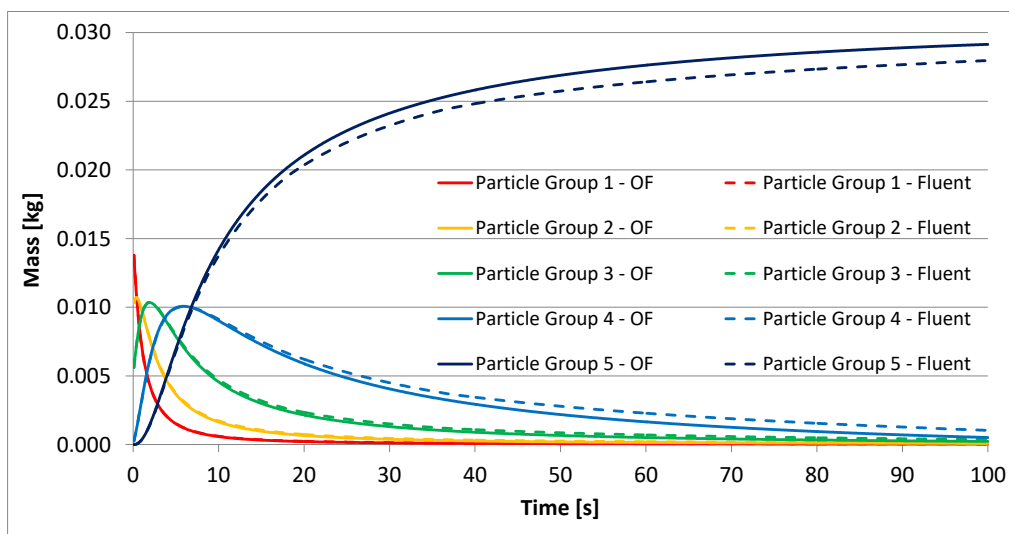
Figure 11 - Total mass of individual particles in the settling column (Fluent and OpenFOAM).

Phase IV – Test Cases for Flocculation and Breakup

To test the implementation of the flocculation and breakup models and to show the relative effects of two different systems, a hydraulic flocculator and a series of mixers were selected. The total volume of each was identical to achieve the same theoretical mean residence time for identical flowrates.

The geometry used for the hydraulic flocculator is presented in Figure 12. This geometry was built based on design guidelines (MWH, 2005) for the purpose of testing the population balance, flocculation

and breakup models. The size of the channels increases through the flocculator in order to reduce the degree of turbulence along the particle trajectory, therefore reducing the possibility of floc breakup.
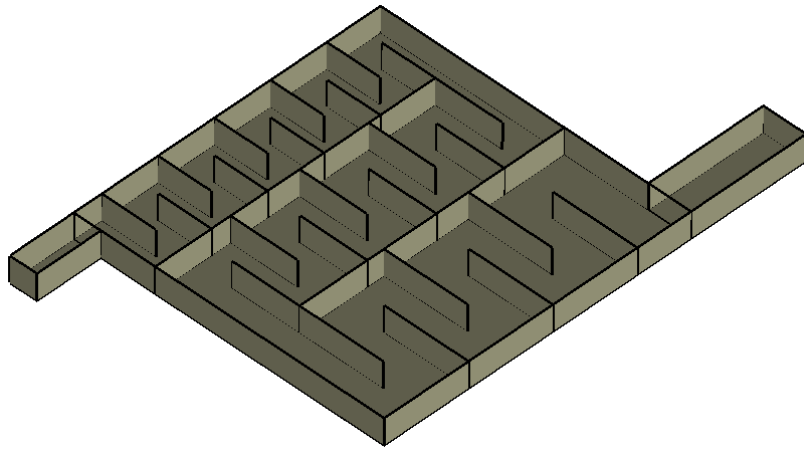
Figure 12 - Geometry for the hydraulic flocculator.

The geometry used for the mechanical flocculator is presented in Figure 13. This geometry was built based on design guidelines (MWH, 2005) for the purpose of testing the models described in this document and consisted of four tanks in series, each with a flat bladed turbine, as shown.


Side view
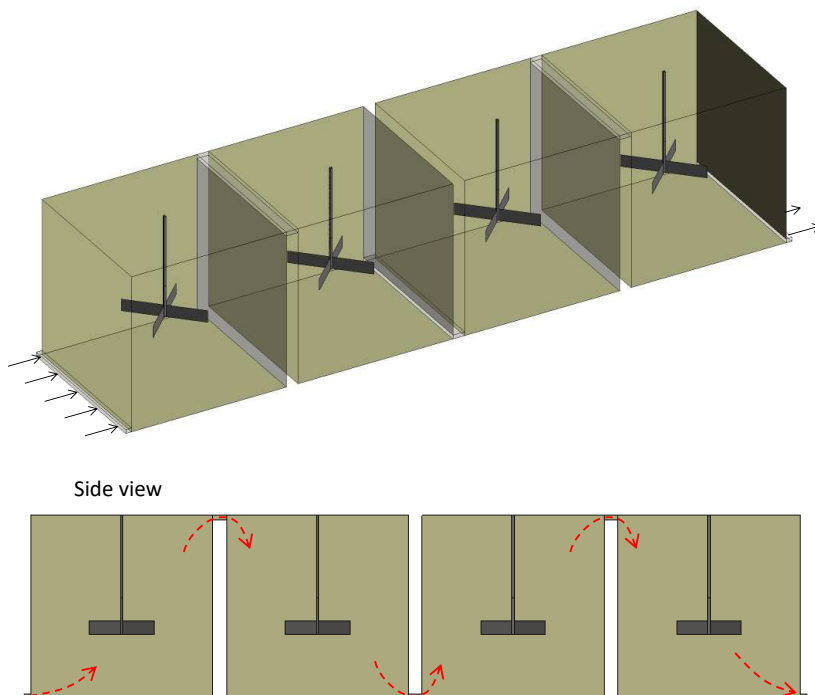
Figure 13 - Geometry for the mechanical flocculator.

Water was specified with a density of 1000 kg/m^3 and a viscosity of 0.00131 kg/ms. Twenty slip scalars were included in the calculation. The density of the particulates was specified as 1005 kg/m^3 and the slip velocity was calculated using a modified Richardson and Zaki (Richardson & Zaki, 1954) model.

Models were included for orthokinetic flocculation and breakup and a collision efficiency was arbitrarily set to 20%.

A qualitative method of assessing design conditions for flocculators is by the Camp number. Figure 14 presents contours of the Camp number for the mechanical and hydraulic flocculators, for comparison, which shows that the Camp number at the outlet is around 30,000 in both cases.
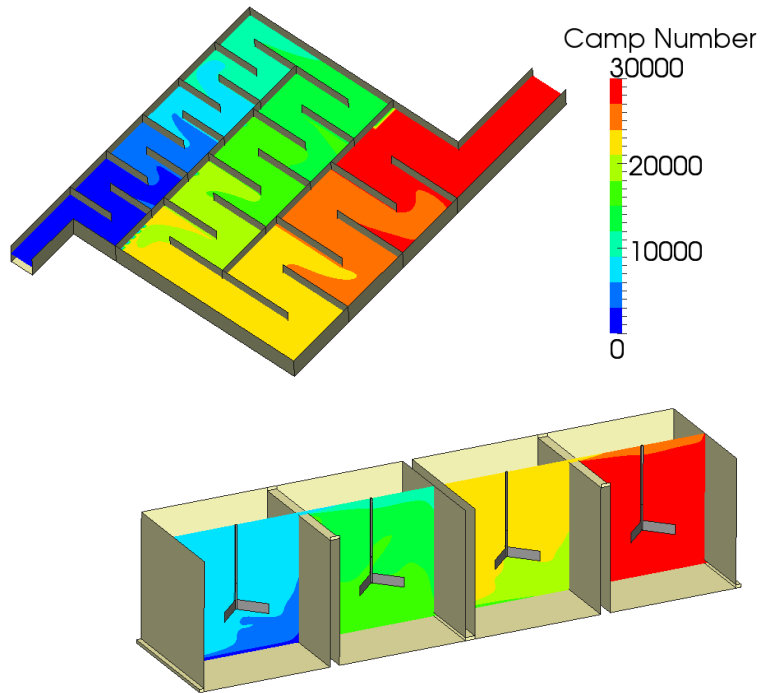
Figure 14 - Contours of Camp number for: top – hydraulic flocculator; bottom – mechanical flocculator.

The results for the particle size distribution suggest that more breakup occurs in the mechanical flocculator compared to the hydraulic flocculator. This comparison is presented in Figure 15. The difference is evidenced by the size distribution being centred on a particle size of 92 µm as opposed to 844 µm in the hydraulic flocculator. Two reasons for this are that (1) the higher values of the G scalar that are present in the mechanical flocculator, as presented in Figure 16, induce floc breakup therefore limiting the maximum floc size and; (2) based on a dye trace experiment, it is seen from the dye trace curve in Figure 17 that there is an earlier break through time in the mechanical flocculator. This is likely to result in particulates passing through without the required exposure time for flocculation to occur.
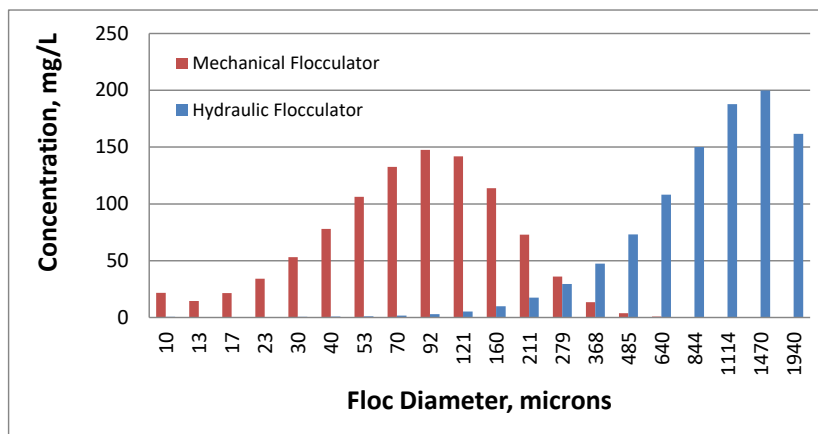
Figure 15 - Particle size distribution for hydraulic and mechanical flocculators.
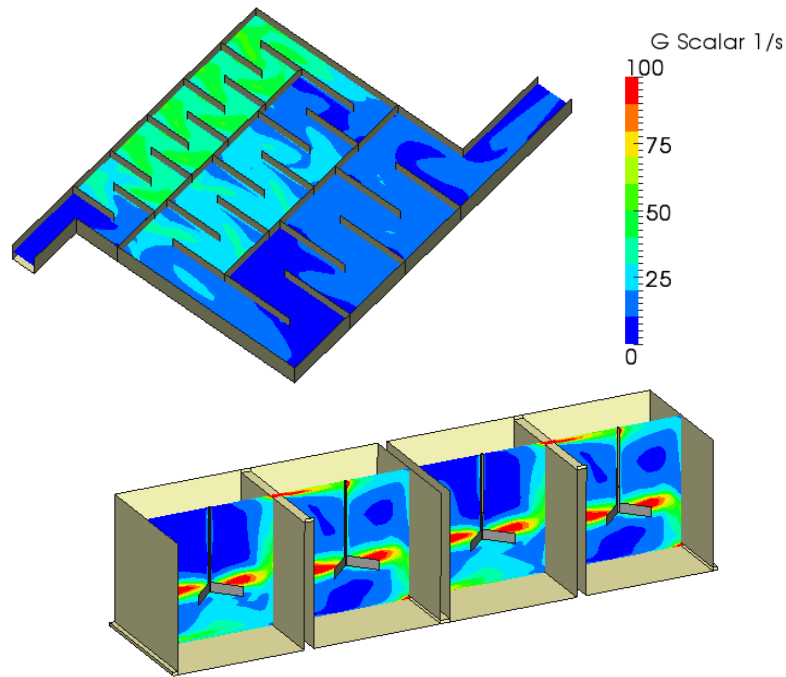
Figure 16 - Contours of G Scalar for: top – hydraulic flocculator (case 4); bottom – mechanical flocculator.
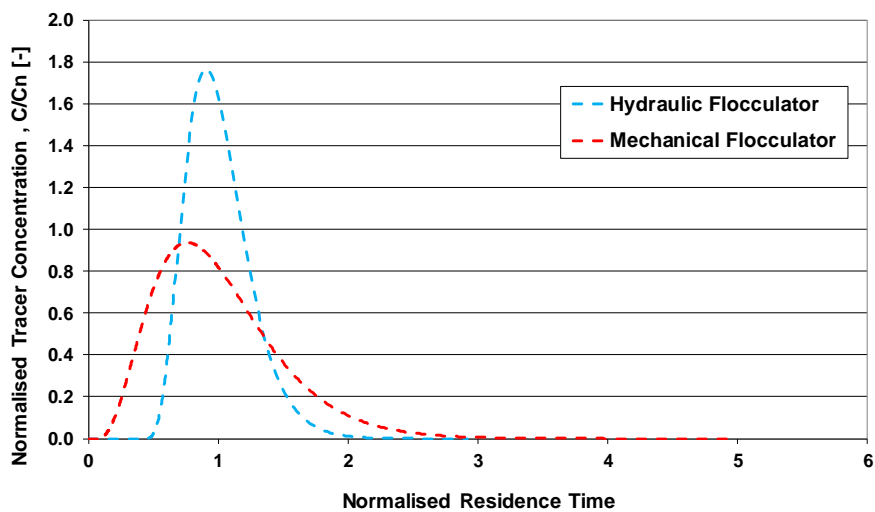

Figure 17 - Dye trace curves for the hydraulic and mechanical flocculators.

## Optimising the Mixing Performance of a Flocculation Tank

Wessex Water were to install a new mixing and flocculation tank at a Sewage Treatment Works. At the time of undertaking the study, Wessex Water had not finalised the design standard.

The study focussed on assessing the hydraulic performance of the tank in terms of mixing and short-circuiting. This was mainly focussed on short-circuiting, as a bypass of solids through the tank may mean particulates would pass through without sufficient residence time for flocs to form.

The work initially assessed a square and circular tank which in these preliminary designs, the floor of the tank was set horizontal. Each flocculation tank was assessed with a Chemineer RL-3 Impeller. The

hydraulic performance was characterised by undertaking dye trace experiments, in addition to comparing the 'G' field and Camp number for each design.

Figure 18 presents a comparison of the circular and square designs that were assessed. The water level was set on each so that there was an identical fluid volume in each tank.
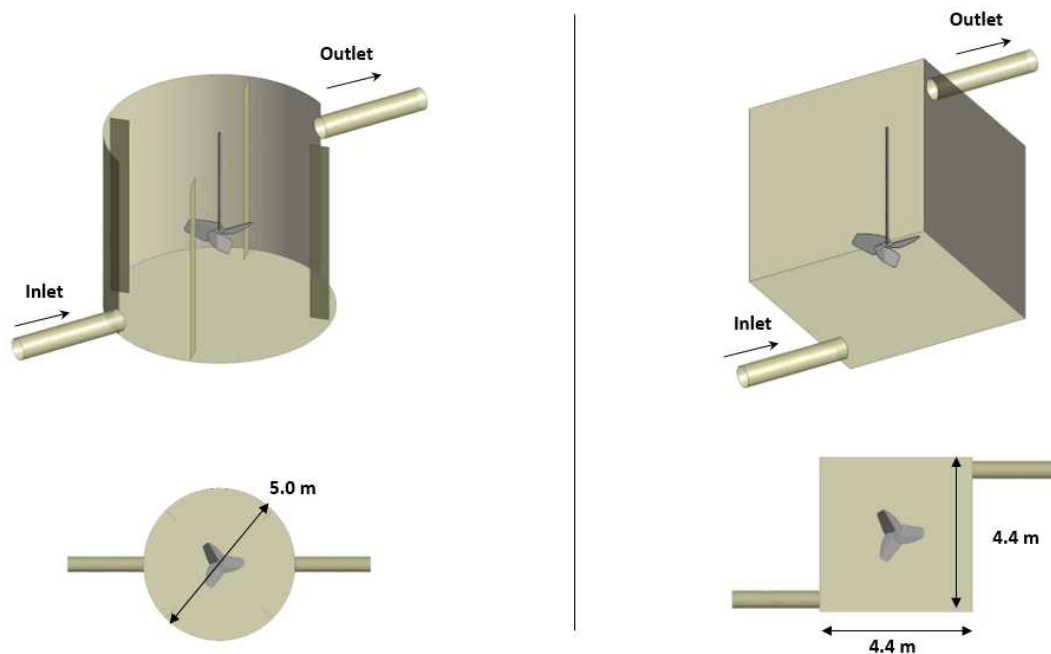
Figure 18. Square and circular flocculation tanks.

It was found that the average 'G' field within the tanks was the same in both cases, with higher shear rates around the impeller, as would be expected. This is presented in Figure 19. However, it was found that, in the square tank, short-circuiting was present, as shown by the spike at the start of the residence time distribution (RTD) plot presented in Figure 20. The short circuiting in the square tank was attributed to the interaction of the inlet flow with the impeller, with the main flow path giving rise to short-circuiting shown by streamlines in Figure 21.

The average Camp number from a hand calculation can be estimated using the following equations and was estimated to be around 26,000.

$$Camp\ No. = G.t \qquad\qquad G = \sqrt{\frac{P}{\mu V}}$$

Where G is the shear rate [1/s], t is time [s], P is power draw from the impeller [W], μ is the dynamic viscosity [kg/ms] and V is the volume [m³]. However, using the local turbulence field from the CFD model in order to calculate 'G', it was found that, for both tanks, the Camp number was around 16,000, which is within the desired range of 10,000 to 100,000, but lower than estimates based on uniform dissipation of the impeller power.
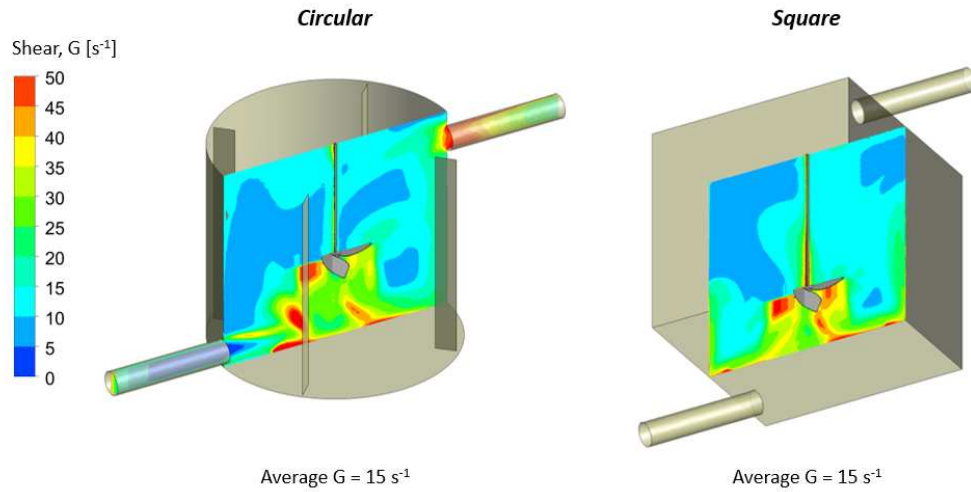
Circular   Square

Shear, G [s⁻¹]

Average G = 15 s⁻¹   Average G = 15 s⁻¹
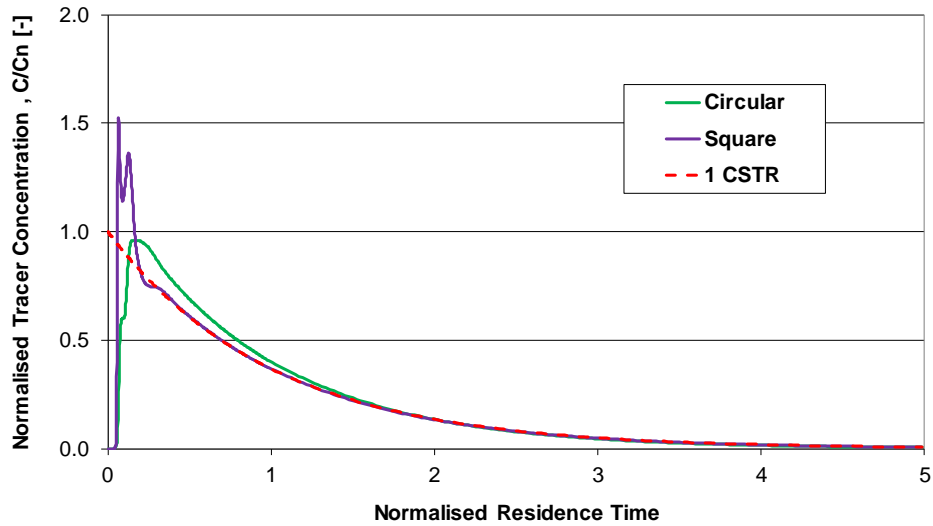
Figure 19. Comparison of 'G' field.

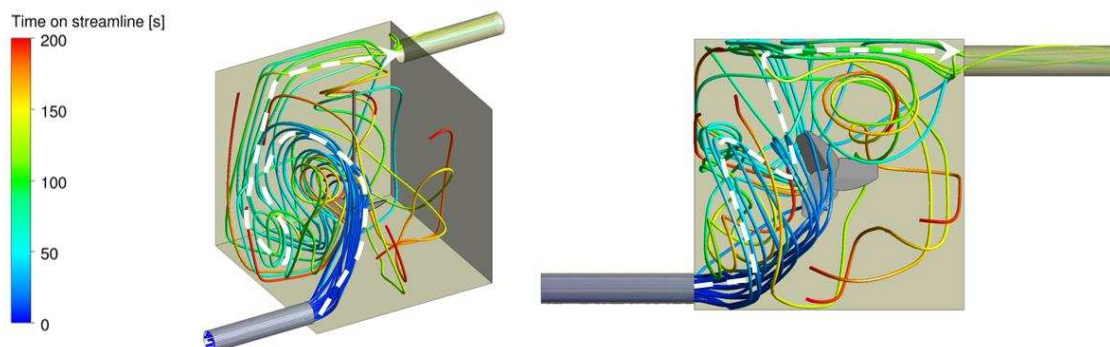**Figure 20. Comparison of RTD for circular and square tanks.**

Figure 21. Streamlines within the square tank, showing the main flow path giving rise to short-circuiting.

As the hydraulic performance of the circular tank was better than the square in terms of short circuiting, the circular tank was selected as the preferred arrangement.

However, some additional changes to the design, mainly a sloped floor to facilitate drainage under a maintenance condition, benching around the circumference of the tank and a representative length of inlet pipe upstream incorporating a 90°bend, resulted in a slight reduction in perform ance, with the RTD showing a little short-circuiting, as presented in Figure 22.

A sensitivity to a weir arrangement on the tank was undertaken, which, as shown by the RTD in Figure 22, was found to reduce short-circuiting, producing an RTD that is a very close representation of a Completely Stirred Tank Reactor (CSTR). This was attributed to 'spreading' the outlet area around the tank so that any dominant flow path towards the outlet was not removed at a point location. A comparison of streamlines for the two cases is presented in Figure 23.
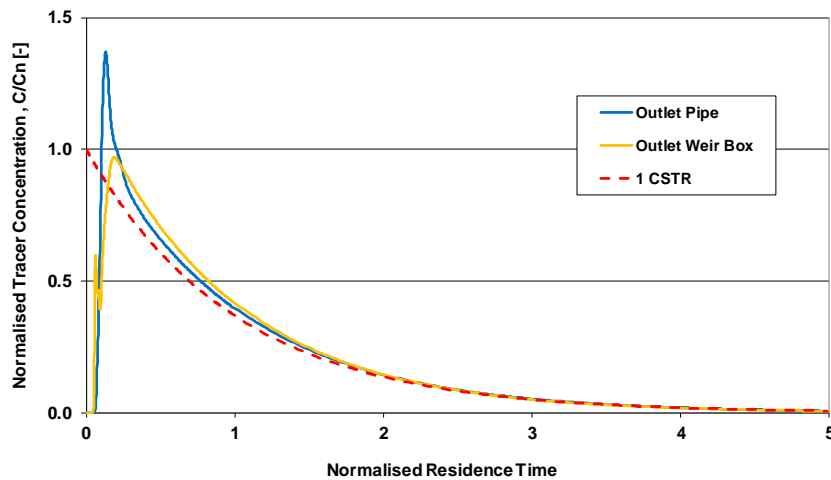

**Figure 22. Comparison of RTD for circular tank with an outlet pipe
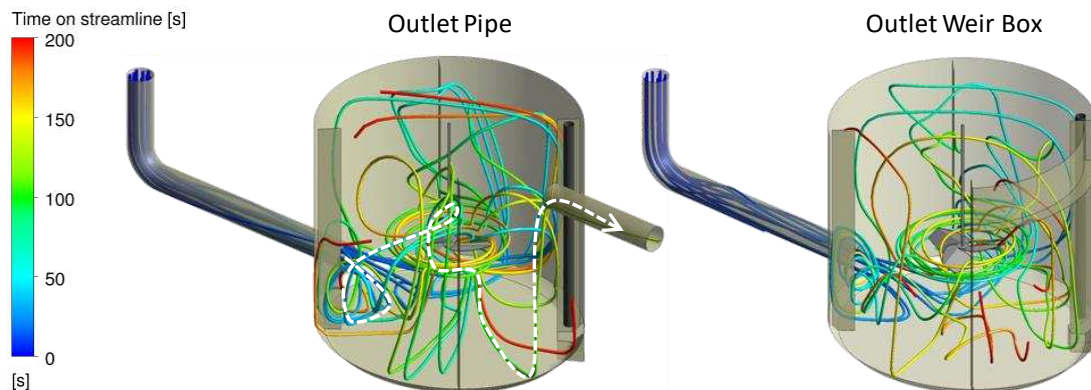and with an outlet weir box.**

**Figure 23. Streamlines within the circular tank with an outlet pipe
and with an outlet weir box.**

Summary

The research programme has resulted in a solver that may be used to calculate flocculation processes. However, challenges remain in acquiring appropriate data, such as initial particle sizes, flocculation efficiency and other empirical constants that are required for the breakup model.

The use of CFD can, however be used to assess a system used for flocculation by assessment of the turbulence or 'G' field to ensure that shear rates aren't too high or low, Camp number to assess the average turbulence and residence time and 'dye trace experiments' to identify whether short circuiting is present, which could result in particulates passing through without sufficient residence time for flocculation to occur. This is an approach that has been pursued by Wessex Water in order to qualitatively optimise a flocculation tank for phosphorous removal.

Acknowledgements

References

Biggs, C. A. & Lant, P., 2002. Modelling activated sludge flocculation using population balances. Powder Technology, Volume 124, pp. 201-211.

Elmaleh, S. & Jabbouri, A., 1991. Flocculation Energy Requirement. Water Research, 25(8), pp. 939 - 943.

Govoreanu, R., 2004. Activated sludge flocculation dynamics: On-line measurement methodology and modelling, Ph.D. Thesis: Universiteit Gent.

Krebs, P., Armbrusterb, M. & Rodib, W., 1998. Laboratory experiments of buoyancy-influenced flow in clarifiers. Journal of Hydraulic Research, 36(5), pp. 831-851.

MWH, 2005. Water Treatment: Principles and Design. New Jersey: Wiley.

Richardson, J. F. & Zaki, W. N., 1954. The sedimentation of a suspension of uniform spheres under conditions of viscous flow. Chemical Engineering Science, Volume 3, pp. 65-73.